Available online at www.sciencedirect.com
ScienceDirect
Acta Materialia 59 (2011) 328–341
Acta MATERIALIA
www.elsevier.com/locate/actamat

A physically based fatigue model for prediction of crack initiation from persistent slip bands in polycrystals

Michael D. Sangid [a], Hans J. Maier [b], Huseyin Sehitoglu [a,*]

[a] Department of Mechanical Science and Engineering, University of Illinois at Urbana-Champaign, 1206 W. Green St., Urbana, IL 61801, USA
[b] Lehrstuhl für Werkstoffkunde (Materials Science), University of Paderborn, 33095 Paderborn, Germany

Received 19 April 2010; received in revised form 18 September 2010; accepted 19 September 2010
Available online 20 October 2010

Abstract

In many engineering applications, fatigue is the dominant failure mechanism governing the life of a component. Thus, many studies have focused on this phenomenon, although there is a need for a model that addresses fatigue based on the material's microstructure, specifically the energetics of the grain boundaries (GBs) and persistent slip bands (PSBs). Our approach is to model the energy of a PSB structure and use its stability with respect to dislocation motion as our failure criterion for fatigue crack initiation. The components that contribute to the energy of the PSB are identified, namely the stress field resulting from the applied external forces, dislocation pile-ups and work-hardening of the material is calculated at the continuum scale. Further, energies for dislocations creating slip in the matrix/precipitates, interacting with the GBs and nucleating/agglomerating within the PSB are computed via molecular dynamics. The results of our simulations on the stability of a PSB produce the correct fatigue crack initiation trends for the grain size, grain orientation, character of the GB, precipitate volume fraction and applied strain. From this information, we see that distinct GBs act as strong barriers to slip and increase the fatigue strength of the material.

Keywords: Fatigue; Grain boundaries; Coincidence site lattice (CSL); Persistent slip bands; Crack initiation

1. Introduction

From experimental results, finer grain material generally experiences a longer fatigue life [1–7], since persistent slip bands (PSBs) are prone to form in larger grains [8–10]. However, previous studies were performed on materials with uniform grain size and cannot address the response of adjacent small/large grains that we account for in the model presented herein. Similarly, there have been a number of studies that examine the grain boundary (GB) character, defined as the density of coincidental atoms between two lattices at the GB, where the density's reciprocal is denoted as the coincident site lattice (CSL) Σ value. Experimental studies have shown that CSL boundaries of high CSL density/low Σ value do not crack during fatigue of Ni [11], stress corrosion of a Ni-based superalloy [12] and cavitation of Cu [13]. Hence, it is important to account for the GB character as this contributes to the formation and stability of a PSB. As a consequence, the affect of individual CSL Σ values on the fatigue behavior of a material as well as the grain size and orientation are addressed in this model.

During the fatigue process, defects multiply and accumulate within the material. This behavior results in an increase in the dislocation density [14]; these dislocations form unique structures in an attempt to minimize the total energy of the system [15]. As a consequence, in many materials strain is localized in the form of slip bands, which are precursors of crack initiation, as first pointed out by Ewing and Humfrey [16], Seeger et al. [17] and Friedel [18]. Persistent slip bands were initially observed in single-crystal face-centered cubic (fcc) pure metals, specifically copper, although the concept has been generalized as a function of temperature,

* Corresponding author. Tel.: +1 217 333 4112; fax: +1 217 244 6534.
E-mail address: huseyin@illinois.edu (H. Sehitoglu).

1359-6454/$36.00 © 2010 Acta Materialia Inc. Published by Elsevier Ltd. All rights reserved.
doi:10.1016/j.actamat.2010.09.036

stacking fault energy, slip character and applied strain amplitude (cycles to failure) [15,19].

Fatigue is distinguished from other types of loading by slip irreversibilities, in which vacancies are generated, creating a flux within the PSB, resulting in surface intrusions and extrusions. Meanwhile, dislocations agglomerate into the walls of a PSB, as a consequence of PSBs being softer than the matrix material, and represent domains of strain localization. Once active, an increase in dislocation density is observed, resulting in hardening of the PSB. Both the hardening behavior and dislocation density are seen to saturate as the fatigue cycling continues [20–22]. Therefore, PSBs represent significant localization of plastic deformation, slip and dislocations, and during this process, hardened (matrix) material forms adjacent to the relatively soft (PSB) regions. The interface between the PSB and matrix is a plane of discontinuity across which there are abrupt strain gradients, resulting in a preferred site for crack initiation [23–25].

Essmann et al. [26] and Differt et al. [27] created a model for extrusions and intrusions resulting from a PSB focusing on randomly distributed irreversible slip processes. Slip irreversibility arises in the material due to dislocation annihilation [26], although dislocation multiplication occurs concurrently, resulting in a dynamic equilibrium within the PSB [28]. This leads to elongation of the PSB, dislocation gliding within the PSB even at low temperatures, extrusions/intrusions at the surface of the single crystal, and an increase in surface roughness. In their model, they estimated the surface roughness which displays a square root dependency on the number of loading cycles [26,27]. This model is physically based and well thought-out. Hence this model serves as an important starting point to us; by including energy barriers, stress fields and an overall energy foundation, we establish a PSB model for crack initiation by integrating perspectives from the atomistic and continuum scales.

Cyclic loading produces positive and negative edge dislocations, which attract each other, forming dislocation dipoles agglomerating in the walls of the PSB that result in a near-zero Burgers vector [29]. Hence, during cyclic loading, dislocations arrange themselves into preferred defect structures to minimize the total elastic strain energy of the system [30,31]. There have been a few attempts to develop a closed-form solution to the stress field developed by the dislocation arrangement of a PSB. Brown used Airy's stress function to develop an expression for the stress field by the dislocations of a PSB [32]. Van der Giessen and Needleman developed a dislocation dynamics model to verify that the stress field from a series of planar edge dislocations can be modeled as a series of hyperbolic terms [33]. Brinckmann extended this model to account for two opposing series of edge dislocations, which provided a good approximation for the dislocation arrangement in a PSB and the resulting stress field [34]. These models represent the stress field of dislocations in a PSB from 2-D dislocation dynamics; hence there is still a need for incorporation of the unique dislocation arrangements within PSBs into a polycrystalline fatigue model, which is addressed in our model.

So fat, we have only discussed PSB formation in single crystals, although dislocation walls and PSBs can form in the most favorably oriented grains within a polycrystalline material [9,35–38]. Lin and Ito developed a model for plastic shear strain accumulation from a PSB in a polycrystal [39]; however, their shear stress field was non-equilibrating. Building on their concepts, in 1981, Tanaka and co-workers created an energy balance of the dislocation structure along the PSB, in order to predict crack initiation [40–42]. Their PSB model consists of two series of dislocations of opposite sign on opposite layers, which account for deformation as a result of forward and reverse loading. From this, Tanaka and Mura wrote a closed-form solution for the number of cycles to failure in a PSB, which can also be expressed in a Coffin–Manson form, which displays a Hall–Petch-type dependency on grain size. Their solution is attractive [43,44] and is comparable to experiments by adding a variable for the degree of irreversibility [45], although there are some concerns and limitations with this model. For instance, it does not take into account the complicated geometry and dislocation arrangement of a PSB and several energy terms need to be incorporated for a complete description of the PSB, including the energetics of the GBs. Further, there is an energy discrepancy as their model takes into account only the portion of the hysteresis loop above yielding.

Historically, the majority of the studies on PSBs have been on pure fcc materials, although PSBs have been observed in alloys [46,47] and superalloys [48–52]. Typically, superalloys are strengthened by an ordered γ' precipitate. Petrenec et al. studied the dislocation arrangements in Ni-based superalloys (IN713 and IN792) at room and elevated temperatures [53–55]. They concluded that persistent slip bands were evident and contained a high density of dislocations. PSBs form as dislocations cut through the matrix and γ' precipitate in a planar slip manner at both temperatures and were the main source of crack initiation [53–55]. Therefore, the PSB structure in precipitate-hardened superalloys (i.e. multiple parallel thin bands) is noticeably different compared to the ladder-like structures observed in single-phase materials.

As previously mentioned, PSB formation manifests in surface roughness by means of intrusions and extrusions. This phenomenon is also seen across the grain boundaries in the bulk of a polycrystalline material [29]. Risbet et al. measured the evolution of extrusions on the surface of cyclically loaded Waspaloy, a Ni-based superalloy using atomic force microscopy [56,57]. The height of a PSB is seen to be nearly zero until a threshold number of cycles is reached, at which point it increases rapidly, and nearly saturates. As expected, this behavior is highly dependent on the applied strain range. In an extremely intensive experimental study, Huang et al. [58] used in situ neutron diffraction to measure the dislocation density in monotonic

and cyclically loaded Hastelloy C-22HS, a Ni-based superalloy. The results show the dislocation density increases during cyclic loading and saturates; as a consequence the mean dislocation spacing decreases as PSBs are formed. The aforementioned work represents an extensive effort in capturing the slip behavior, dislocation density, wall spacing, PSB height and extrusion length evolution with number of cycles during fatigue of Ni-based superalloys; these quantitative values and trends are extremely valuable for use in this study.

Persistent slip bands have been examined in detail over the last 30 years, but a model capturing its complexities has yet to emerge. In this study, we formulate a model for predicting fatigue crack initiation in a wrought Ni-based superalloy, although this methodology could be used to characterize fatigue in a variety of metals and alloys. This material was chosen due to the complexities and wide distributions of microstructural features, further validating our model. Hence, we establish a physically based fatigue model that incorporates the microstructure (grain size, grain orientation, GB character and γ' distribution) and the unique nature of fatigue dislocation structures, i.e. PSBs. The model encompasses continuum and atomistic contributions in a unified energy expression. In the subsequent sections each component contributing to the overall energy of the PSB section are identified and quantified. These components are the heart of our fatigue model, which establishes an energy balance for a PSB.

2. Material characterization

The material utilized in this study is a Ni-based superalloy, Udimet 720 (U720). The primary strengthening mechanism in this material is in the form of ordered Ni_3Al precipitates ($L1_2$ structure), which occur in this material at three length scales (primary, secondary and tertiary). The coherency of these γ' precipitates with respect to the γ matrix offers stability along with enhanced strengthening at elevated temperatures. The material underwent a solution process at 1100 °C for 2 h followed by oil quenching, in order to prepare the matrix for uniform precipitation of γ'. Afterwards, it was aged at 760 °C for 8 h with air-cooling, in order to precipitate the coarser γ', which offers creep resistance. A second aging process at 650 °C for 24 h with air-cooling produced fine γ', thus strengthening the microstructure for tensile and fatigue loads and stabilizing the γ' precipitates.

Also, during the heat treatment process the γ' acts to pin the grain boundaries, thus determining the grain size in the γ matrix. In this material, there are areas of densely populated γ' along side areas denuded of γ', as shown in Fig. 1a. As a result, there exists a wide distribution of grain sizes, as fine grains form in regions of heavily populated γ' and coarse grains form in regions where γ' is sparse. Data on grain size and orientation were obtained from electron backscatter diffraction (EBSD) scans. The mean grain area is 4 μm^2, although grains can reach over 100 μm^2 (Fig. 1b). The long tail of the grain size distribution and dual peaks shown in Fig. 1b suggest a bimodal-like distribution of grain sizes with large variations. Further, due to the variation in grain sizes and neighboring grains, each grain can have a wide distribution of associated GBs. From this analysis, the CSL values of the GBs within each specimen and the energy of each individual GB were determined by the methodology described in Ref. [59] and shown in Fig. 2a and b, respectively.

In this study, strain-controlled experiments were conducted on U720 fatigue specimens at 1.3% and 0.9% total

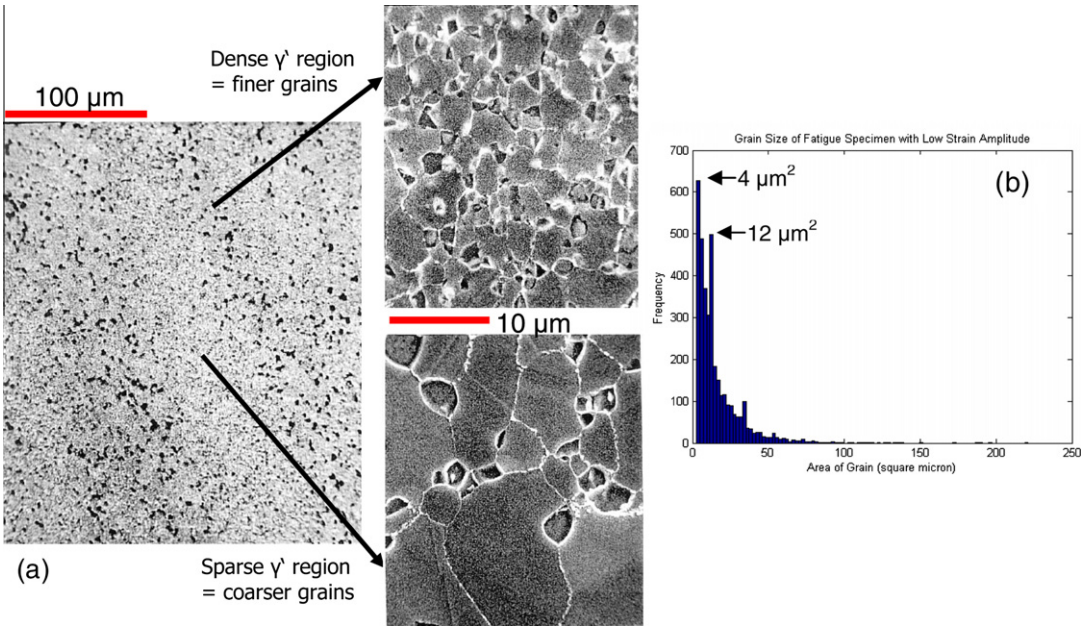

Fig. 1. (a) Microstructure of U720, displaying bands of γ' precipitates (left). These precipitates determine the grain size. In areas of densely populated γ', the grain size is fine, while in areas denuded of γ', the grain size is coarse. (b) Histogram of the grain area from a 2-D EBSD scan.

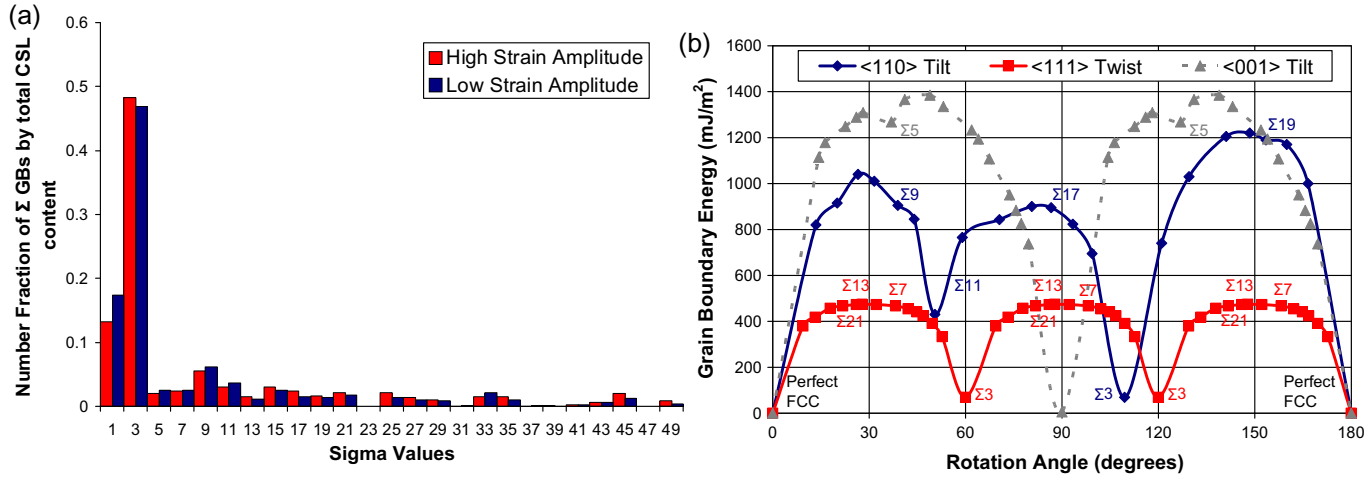

Fig. 2. (a) Histogram of CSL values for specimens of U720 after fatigue testing at 538 °C. (b) The grain boundary energy shown as a function of the rotation angle for nickel in the ⟨1 1 0⟩ tilt, ⟨1 1 1⟩ twist, and ⟨0 0 1⟩ tilt directions.

strain ranges at 538 °C and $R_\varepsilon = 0$. During reverse cycling, the specimens experience considerable compressive plasticity; thus we believe the PSB behavior in our strain-controlled experiments (strain ratio $R_\varepsilon = 0$) is comparable to stress-controlled fully reversed studies ($R = -1$) in the literature. Interestingly, the character of the GBs remained constant during fatigue testing, regardless of the applied strain amplitude. The fracture surfaces of failed fatigue specimens were analyzed to study the mechanism for crack initiation, as shown in Fig. 3a and b. Transgranular failure is observed and is of primary interest in this study. Material characterization in the form of transmission electron microscopy (TEM) was performed, which provided a qualitative indication of the material behavior, thus providing key insights that can be used to model the microstructure and resulting dislocation arrangements. As expected, noticeably different dislocation arrangements form during monotonic and cyclic loading [15,19]. In the fatigued samples, slip and plastic strain are localized into banded regions. Fig. 3c shows a detailed TEM image of two slip bands in U720, and a low-magnification view of persistent slip bands is shown in the inset. Similarly, the observation of persistent slip band formation has been observed in the literature for U720 [60–62] and is the precursor to crack initiation and material failure.

From this TEM analysis, we draw many insights into the strain localization that ultimately leads to failure within U720. The formation of the persistent slip bands occurs in preferentially oriented grains. Slip interacts with the GB causing pile-up of dislocations and stress concentration, which results in slip penetrating into the second grain. By viewing the high-magnification image, we see that the slip band forms by dislocations shearing the γ' precipitates. This effectively weakens the precipitate as an obstacle for future dislocations to penetrate (cutting reduces the effectives size of the precipitate and the ordering of the Ni_3Al intermetallic structure) and concentrates plastic deformation into a small volume. This results in slip being confined to a single glide plane (a 2-D planar feature). Initially one slip band forms as the precipitates are cut at the weakest spot, since this alloy has a statistical distribution of local strength (i.e. interparticle distances). However, the increase in dislocation density hardens the slip band, and thus cutting sets in at the next weakest plane. Consequently, we get an increasing number of slip bands with cycle number, but not much change within the bands, which macroscopically results in cyclic saturation.

3. Modeling and results

Our approach is to model the energy of a PSB structure, E, and use its stability with respect to dislocation motion as our failure criterion for fatigue crack initiation. The concept of an energy balance and stability of a dislocation structure within a material is not new; it has a long-standing historical basis [40–45,63–67]. Moreover, this approach allows us to address the small length scale problems via incorporation of atomistic simulations. Hence, the atomic simulations provide important insights into the energy barriers and physics of the grain boundaries, which are crucial to fatigue of a polycrystalline material. All the contributing energy factors to the PSB are addressed and our energy balance is as follows:

$$\begin{aligned} E = & -E^{\sigma}_{app}(\sigma, m, L, N) - E_{hard}(\rho, L, N) \\ & + E^{disl}_{pile-up}(h, d, L, N) + E^{disl}_{nuc}(m, \Sigma, h, L, L', N) \\ & + E^{slip-GB}_{extrusion}(m, \Sigma, h, L, L', N) + E_{APB}(L, \gamma'_{dist}, N) \\ & + E_{\gamma-SF}(L, \gamma'_{dist}, N), \end{aligned} \tag{1}$$

where σ is the applied stress during fatigue loading, N is the number of cycles, m is the Schmid factor of the grain containing the PSB, L is the grain size, L' is the size of the neighboring grain, h is the height of the PSB, d is the mean dislocation spacing within the PSB, ρ is the dislocation density within the PSB, Σ is the character of GB in the CSL, and γ' is the

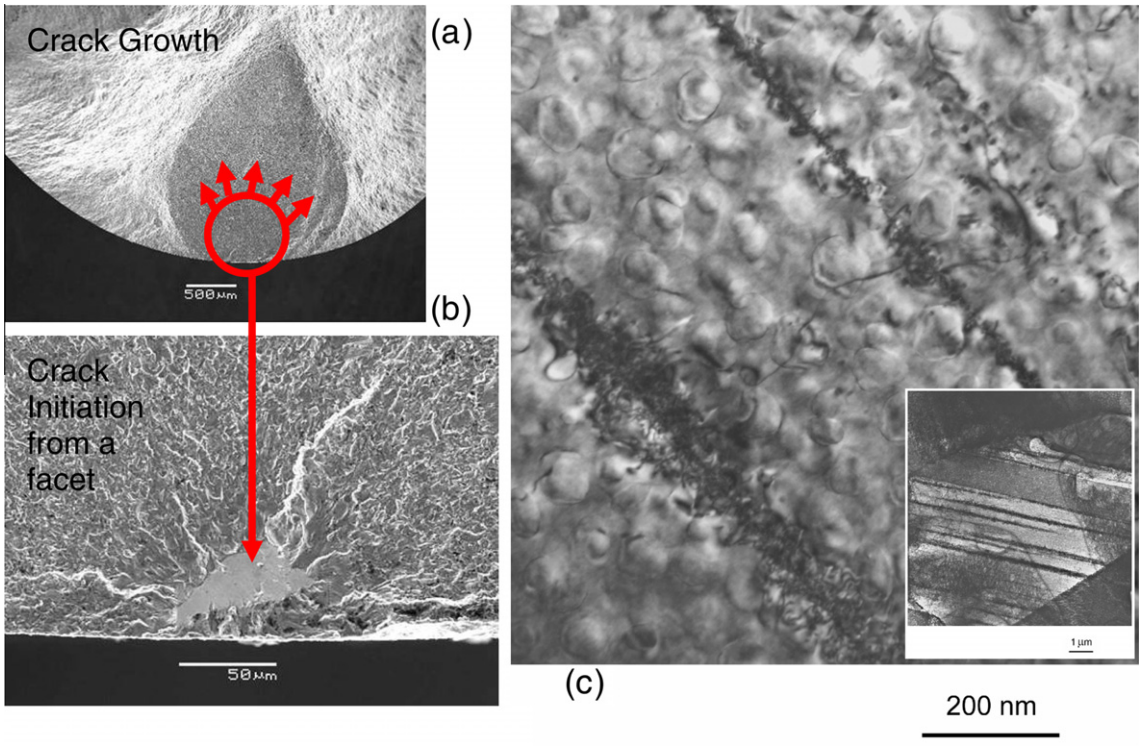

Fig. 3. (a) Fracture surface of a failed fatigue specimen. (b) A crack initiates from a transgranular facet, although considerable plasticity is involved in forming this feature. (c) A high-magnification image of two slip bands in a failed fatigue specimen of U720 tested at 1.3% strain range, $R = 0$ and 538 °C. A low-magnification TEM image of PSBs is shown in the inset.

distribution of Ni_3Al precipitates. The first three terms of the energy expression are associated with the continuum length scale, and other terms are derived by atomic simulations. Each term will be discussed in the subsequent sections.

The geometry of the PSB within the most favorably oriented grain of a polycrystal is shown in Fig. 4a, which shows that the dislocations localize into the PSB and form wall structures. The PSB intersects the GB; as a consequence of slip within the PSB, extrusions are formed across the GB. Extrusions were originally defined for slip emanating at surfaces; however, PSB impingement at grain boundaries can also constitute crack initiation [8]. In this case, as Mughrabi et al. has shown [29] (Fig. 4b), interactions between PSBs and GBs in polycrystals result in a static extrusion, resulting in ledges/steps, thus roughening the GB. The number of dislocations within the extrusion is given by $n_{dis}^{pen}\vec{b}h$, where n_{dis}^{pen} is

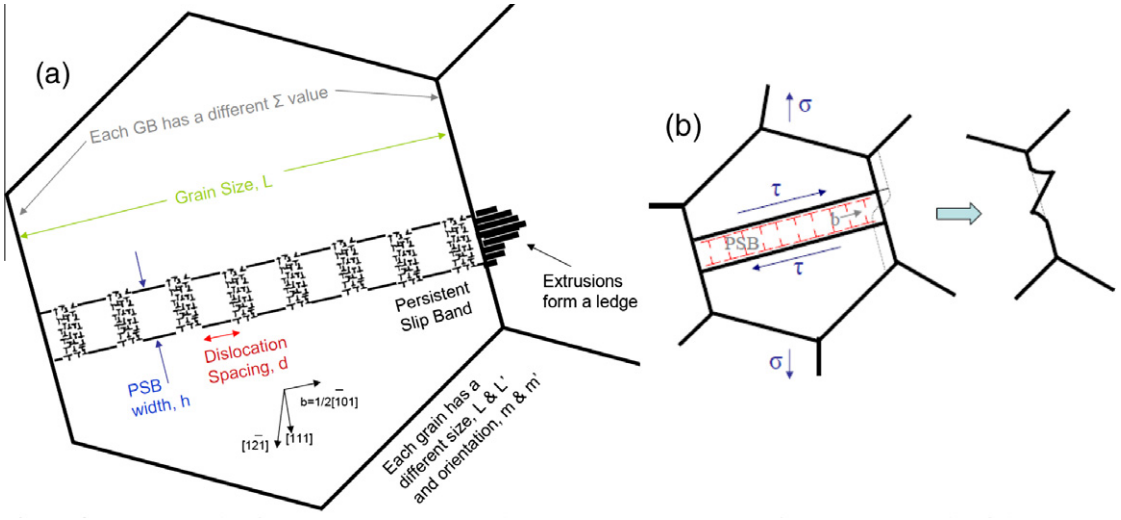

Fig. 4. (a) Schematic of the PSB geometry (h, d) in the polycrystal. The PSB forms across a grain of size L and orientation (Schmid factor, m) and intersects a pair of GBs each with an associated Σ value. (b) Extrusions form across the GB. Although extrusions were originally defined as being due to PSBs causing slip at a free surface, interactions of a PSB with GBs leads to static extrusions across the GB in the form of ledges and steps. Redrawn from Ref. [29].

the number of dislocations that penetrate the GB on a single slip plane and $\boldsymbol{b}$ is the Burgers vector.

3.1. Continuum terms

The continuum terms (the first three terms in Eq. (1)) create an internal stress field, in which the glissile dislocations must overcome this stress field to plastically deform the material [68] by an increment of slip, ∂X, as follows:

$$E_\tau = \bar{\tau}\vec{b}Ln^{layers}\partial X, \tag{2}$$

where the overall shear stress, $\bar{\tau}$, is composed of the dislocation field in the PSB structure, τ^{dis}, the work-hardening of the system, τ^h, and the external applied resolved shear stress, τ^A.

$$\bar{\tau} = \tau^{dis} - \tau^h - \tau^A. \tag{3}$$

It is paramount to account for each layer of successive dislocations that are gliding with the PSB. The number of moving planes within the PSB is quantified by n^{layers}, which is related to the PSB width, h:

$$n^{layers} = h/\vec{b}. \tag{4}$$

The width of the PSB, h, was measured from the TEM images of U720 (e.g. Fig. 3c). This quantity was seen to increase according to a square root function with increasing number of cycles, and then saturate. The individual stress components that contribute to the internal stress field are discussed next.

3.1.1. Dislocation pile-up

Within the PSB, dislocations agglomerate and form dipole structures, in order to minimize their total energy, as shown in Fig. 4. The dipole structure within the PSB can be modeled as layers of opposing signed dislocations [26,39,40] separated by a distance, h. Within each layer is a series of dislocations, equally spaced by d. In doing so, we can assume linear elastic, isotropic, plane strain behavior, thus greatly simplifying the problem, in order to find the stress within the PSB. The stress field created by the dislocation dipoles within the PSB is given by τ^{dis} as it varies spatially (x, y) within the PSB [34]:

$$\tau^{dis} = \frac{\mu b\pi}{(1-\nu)d^2}\left(\frac{y\left(1-\cos\left(\frac{2\pi x}{d}\right)\cosh\left(\frac{2\pi y}{d}\right)\right)}{\left(-\cos\left(\frac{2\pi x}{d}\right)+\cosh\left(\frac{2\pi y}{d}\right)\right)^2} - \frac{(h+y)\left(1-\cos\left(\frac{2\pi x}{d}\right)\cosh\left(\frac{2\pi(h+y)}{d}\right)\right)}{\left(-\cos\left(\frac{2\pi x}{d}\right)+\cosh\left(\frac{2\pi(h+y)}{d}\right)\right)^2}\right), \tag{5}$$

where the elastic constants μ, ν are the shear modulus and Poisson ratio at elevated temperatures (538 °C), respectively. The resulting contour plot of the stress field due to dislocation pile-ups within the PSB is shown in Fig. 5. The mean dislocation spacing, d, is determined based on the dislocation density within the PSB, ρ, as follows:

$$d = \frac{1}{\sqrt{\rho}}. \tag{6}$$

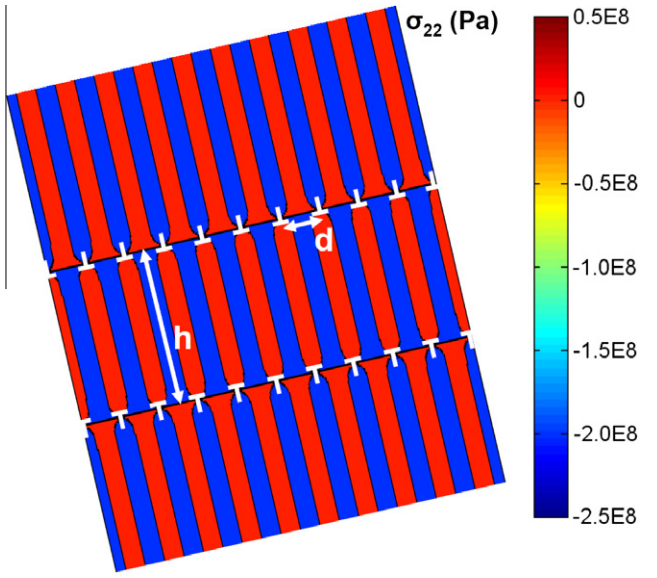

Fig. 5. Contour plot of the stress field in a PSB (height h) from the dislocation dipole walls (separated by a distance d, as shown in the schematic in Fig. 4). The PSB is modeled as two alternating layers of edge dislocations separated by h containing a series of dislocations with spacing d.

In Eq. (5), the dislocation pile-up stress is given as a function of spatial position. It is of particular interest to understand which value is pertinent to our study. In previous models, Mura et al. [40–45] and Brinckmann [34] described failure for a PSB as a crack breaking apart the material in the middle of two opposing dislocation series, although this approaches the material's cohesive strength and refers to a more brittle mode of fracture. Another theory is the existence of a significant gradient in the strain field at the junction between the relatively soft matrix and a heavily work-hardened PSB, resulting in crack initiation at this junction [24,25]. From the latter theory, the stresses near the top and bottom of the slip band are most significant to our model.

3.1.2. Work-hardening

As previously mentioned dislocations shear a given precipitate and weaken the effective area of the particle, which makes it easier for subsequent dislocations to cut the particle on the same slip plane. The dislocations accumulate and interact with each other, resulting in significant work-hardening within the PSB [17,18,20,28,58]. This work-hardening can relax in many ways the elastic stored energy during cyclic loading. Hence, it must be taken into account. In this model, the work-hardening is assumed to follow a Taylor relationship:

$$\tau^h = \alpha\mu b\sqrt{\rho} + \tau_o, \tag{7}$$

where the scalar, $\alpha = 0.45$ [69]. The initial shear stress, τ_o:

$$\tau_o = \frac{\sigma_y}{M}, \tag{8}$$

is given by the yield stress at the test temperature normalized by the Taylor factor, M, which is nearly random (3.16)

for this material. The evolution of dislocation density with loading cycles (N) was extracted from the literature for a similar Ni-based superalloy studied by Huang et al. [58] and a power law was used to fit the data, $F(N)$:

$$F(N) = A_1 N^{c_1} + A_2. \tag{9}$$

Since Huang's study only represents one test condition, the functional form of the dislocation density was amended by the following ratios for each variable:

$$\rho \propto \frac{(\gamma^{pl}_{ratio})^2 (m_{ratio})^2}{\exp(E^{\gamma-nuc-GB}_{ratio})} \cdot F(N). \tag{10}$$

The relationship for the Schmid factor, m, and dislocation density is derived from simple expressions for the Taylor hardening and inelastic strain rate, respectively:

$$\tau = m\sigma = \alpha\mu b\sqrt{\rho} \Rightarrow \rho \propto m^2. \tag{11}$$

Similarly, by relating the Orowan equation to the inelastic strain rate, an expression between the dislocation density and activation energy is developed:

$$\dot{\gamma} = \vec{b}\rho\bar{v} = \dot{\gamma}_o \exp\left(\frac{-\Delta E}{kT}\right) \Rightarrow \rho \propto \exp(-\Delta E). \tag{12}$$

Due to the volatile nature of the exponential term, a Taylor expansion was used to the second power. The plastic strain amplitude relationship was verified by experimental data by Grosskreutz [20] for the dislocation density in copper single crystals as a function of shear flow stress, which can be related to the plastic shear strain as follows:

$$\rho \propto (\gamma^{pl})^2. \tag{13}$$

3.1.3. Applied stress

The applied shear stress for each grain, τ^A, is measured from the hysteresis behavior of the material during the strain control test and multiplied by the Schmid factor of the individual grain, m.

$$\tau^A = m \cdot \Delta\sigma^A = m \cdot H(N). \tag{14}$$

The evolution of alternating stress during loading, $\Delta\sigma^A$, is obtained from the test data on the polycrystalline material, which in this study is a Ni-based superalloy, U720. The stress response, $H(N)$, resembles a square root function as it hardens with increasing number of cycles and saturates. The stress is dependent on the applied strain, although at each strain range, the stress saturates after approximately 100 cycles.

3.2. Atomistic contributions

During the fatigue process, dislocations nucleate and shear the γ' precipitates to form shear bands. Once formed, the dislocations within the PSB interact with the GB. In order to capture the physics at the GB interface, it is necessary to investigate this problem at a smaller scale. Hence, atomic simulations in the form of molecular dynamics (MD) are utilized and the results are incorporated into the energy balance in the form of energy barriers. This approach allows us to address the problems at hand and leverage our atomistic simulations, such that we do not encounter the inherently high stresses associated with MD. The following sections address the four last terms in Eq. (1).

3.2.1. Dislocation nucleation from GB and agglomeration in the PSB

Dislocations nucleate during fatigue loading and agglomerate in the PSB, resulting in a hardening response. GBs act as distinct sources for dislocations. Depending on the character of each GB, there is a different energy barrier for dislocation nucleation from the GB. As discussed in the Appendix A and in greater detail in Ref. [70], it was shown that the energy barrier to nucleation, $E^{\gamma-nuc-GB}_{MD}$, is inversely related to the static GB energy, E^{GB}_{Static}, through a power-law relation (Fig. 6a):

$$E^{\gamma-nuc-GB}_{MD} = 6.0 \times 10^{15} \cdot (E^{GB}_{Static})^{-1.3}. \tag{15}$$

Hence, GBs with stable configurations and low interface energy have a larger energy barrier to nucleating a dislocation. With this information, we can model the energy associated with the nucleation of dislocations from a distinct GB as:

$$E^{disl}_{nuc} = \sum_i \partial X_i \cdot E^{\gamma-nuc-GB}_{MD}(\rho - \rho_o)\vec{b}hL^2. \tag{16}$$

The number of dislocations nucleating within the PSB during loading is represented by the evolution of dislocation density within the PSB multiplied by the cross-sectional area of the PSB: $(\rho - \rho_o)hL$. This energy contribution is dependent on the individual slip increment, ∂X_i, for movement of a dislocation after nucleation.

3.2.2. Dislocation–GB interactions to form extrusions

As previously mentioned, dislocations glide within the PSB and as a result the dislocations interact with the GB. Depending on the character of the GB, there are different energy barriers to dislocations penetrating the GB. Once again, this value is specific to the CSL Σ value (Appendix A and Ref. [70]), as measured from MD simulation, as shown in Fig. 6b. The relationship between the energy barriers for a dislocation to penetrate the GB, $E^{\gamma-slip-GB}_{MD}$, and the static GB energy is given by:

$$E^{\gamma-slip-GB}_{MD} = 2.8 \times 10^{13} \cdot (E^{GB}_{Static})^{-0.6}. \tag{17}$$

In cases where the dislocations penetrate the GB, the PSB forms an extrusion across the GB, as shown in Fig. 4. The intersection between the PSB and GB is a preferred site for crack initiation as pointed out by Mughrabi et al. [29] and Blochwitz and co-workers [8]. Thus, we must account for the energy in the formation of a static extrusion at the GB of the polycrystal; hence the associated energy with the PSB forming an extrusion (step/ledge features) at the GB is of the form:

$$E^{slip-GB}_{extrusion} = \sum_i \partial X_i \cdot E^{\gamma-slip-GB}_{MD} n^{pen}_{dis}\vec{b}h, \tag{18}$$

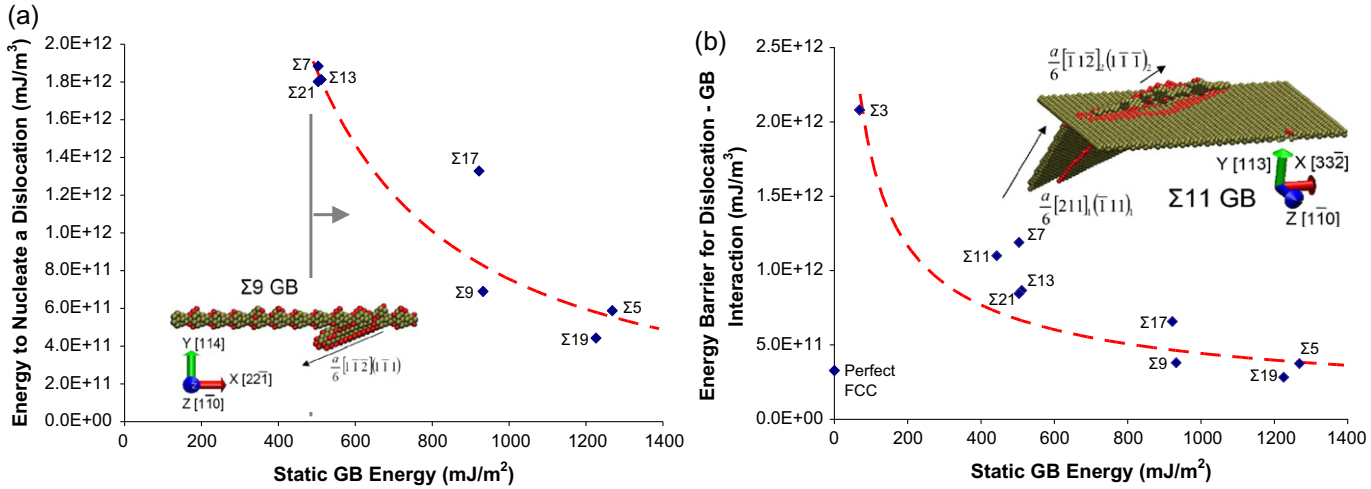

Fig. 6. (a) Energy barriers for slip to nucleate from a GB plotted against the static GB energy for various types of Σ CSL value GBs. The data range is only valid to the right of the gray solid line, since dislocations did not nucleate at the GB in cases of low GB energy in the MD simulation. (b) Energy barriers for slip to penetrate a GB plotted against the static GB energy. In each plot, there is a relationship between the static GB energy and GB energy barrier as shown by the power-law fit of the data (red dash line). (For interpretation of the references to colour in this figure legend, the reader is referred to the web version of this article.)

where n_{dis}^{pen} is the number of dislocations that penetrate the GB. This quantity can be approximated based on the AFM measurements of extrusions at the surface of a Ni-based superalloy by Risbet et al. [56,57]. In their study, they measured the height of the extrusions, which we normalize by the Burgers vector, $\boldsymbol{b}$, to obtain n_{dis}^{pen}. The extrusion height was measured as it evolved with increasing load cycles for various applied strain ranges. After a threshold number of loading cycles, N_{th}, the extrusions appeared and were pronounced; as expected, extrusions are observed after fewer cycles at higher applied strain ranges compared to lower strain ranges. The functional format, $G(N)$, used to fit this data is a square root dependency, based on models of Essmann et al. [26] and Differt et al. [27] of surface roughness:

$$G(N) = A_2\sqrt{N - N_{th}}. \tag{19}$$

Once again, the values of the AFM measurements must be normalized to account for different microstructure conditions; hence n_{dis}^{pen} is proportional to the following ratios:

$$n_{dis}^{pen} \propto \frac{(\gamma_{ratio}^{pl})^2 (m_{ratio})^2 (L_{ratio})}{\exp(E_{ratio}^{\gamma-ext-GB})} \cdot G(N), \tag{20}$$

where the plastic strain ratio is confirmed by the experiments of Risbet et al. [56] and the theory by Mughrabi et al. [29], and the grain size dependency is derived by the irreversible slip in a PSB model by Risbet et al. [57]. Similar arguments were made for the Schmid factor and activation energy dependence as aforementioned in Eqs. (11) and (12), respectively. By taking into account the activation energy of the GB, we can effectively modify Risbet et al.'s AFM measurements of the extrusion height at the free surface to quantify the static extrusions across GBs.

3.2.3. Dislocations shearing the matrix and γ′ precipitates to form PSBs

The preceding sections addressed modeling PSBs in general terms; here we refer to the case of superalloys investigated in this study. Thus, the mechanism for slip band formation in this material by cutting through the γ matrix and the γ′ precipitates is discussed, as shown in Fig. 7a. In order to do so, the dislocation must overcome an associated energy based on the glissile dislocation destroying the (fcc) lattice stacking sequence (Fig. 7c) in the γ matrix and stacking sequence and order in the γ′ precipitates as shown in Fig. 7d and e, which correspond to the stacking fault, γ_{SF}, and anti-phase boundary, γ_{APB} (APB) energy, respectively. Various types of γ′ precipitates form in these complex alloys; however, all are basically the same with respect to the issue of slip localization and shearing. Based on the composition of U720 and our characterization, we see the majority of the precipitates are comprised of Ni_3Al. For the sake of brevity, we model the γ′ precipitates as Ni_3Al, which are in an ordered $L1_2$ structure; thus the ordering of the Ni and Al atoms within the lattice creates the additional obstacle to slip. Hence, the energy associated with the formation of the PSB from shearing the γ matrix and the γ′ precipitates is given by:

$$E_{APB} + E_{\gamma-SF} = \left(f\int_o^L \gamma_{APB}dL + (1-f)\int_o^L \gamma_{SF}dL\right) n_{eff}^{layers}\partial X, \tag{21}$$

where f is the volume fraction of γ′ precipitates and n_{eff}^{layers} is the number of effective layers contributing to the stacking fault or APB energy, as each additional layer provides 95% of the energy value of the prior layer. For U720, the fraction of γ′ precipitates is approximately 0.20 as shown in Fig. 7b by the use of image analysis software on optical micrographs.

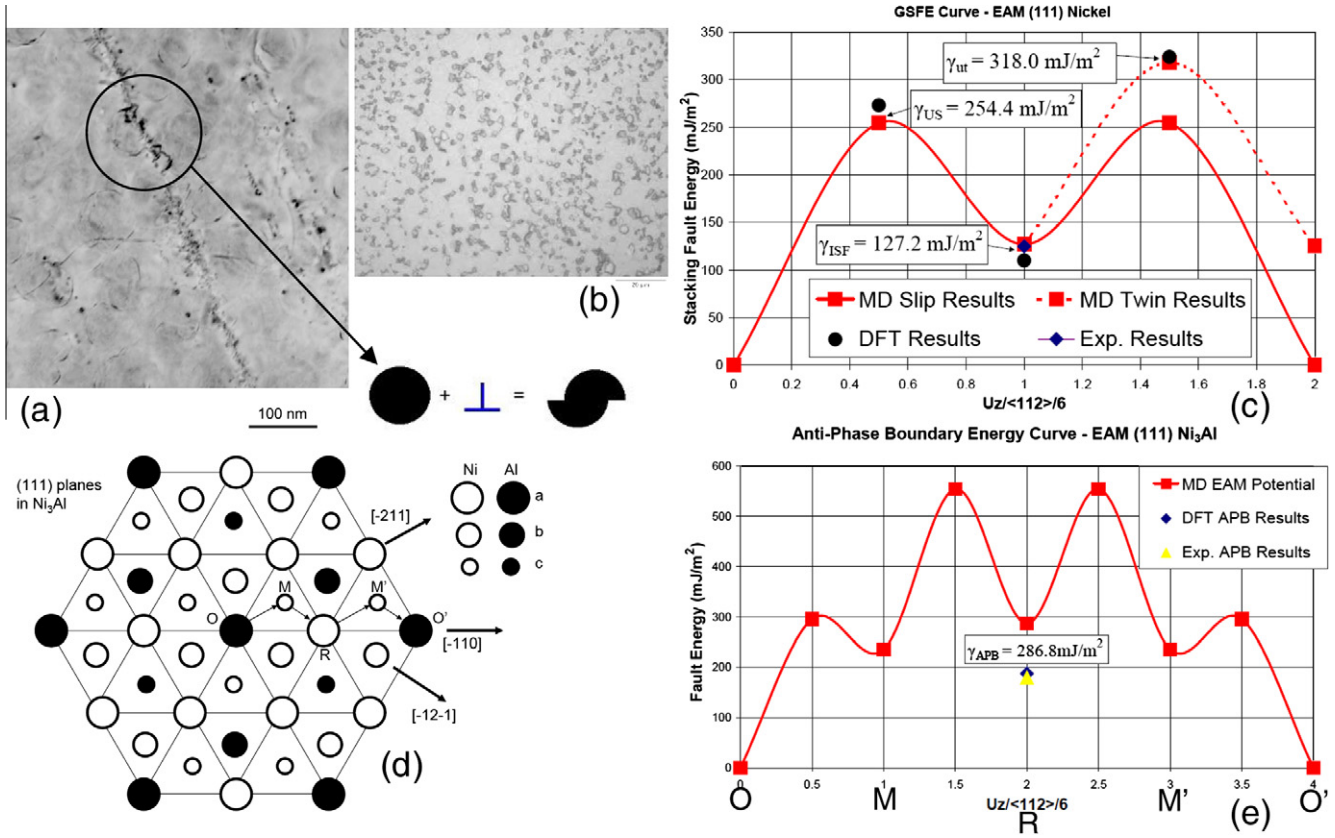

Fig. 7. (a) Dislocations shearing the γ' precipitates, which is necessary to form slip bands. g/3 g weak-beam image shown with contrast inverted. (b) Optical image of U720, displaying the γ' precipitates (fraction ≈ 0.20). (c) Generalized stacking fault energy (GSFE) curve, which corresponds to the energy pathway for slip in the matrix material. (d) Schematic of the ordered Ni_3Al γ' precipitates; redrawn from Ref. [74]. (e) The corresponding energy pathway that must be overcome to penetrate the precipitate, also referred to as the anti-phase domain boundary energy (APB).

An embedded atom method (EAM) potential for Ni [71] was chosen to match the intrinsic, γ_{ISF}-127 mJ m^{-2}, and unstable, γ_{US}-255 mJ m^{-2}, stacking fault energies of the material (Fig. 7c), which compares well with experimental values of 125–128 mJ m^{-2} and ab initio calculations of 273 mJ m^{-2} for the γ_{ISF} and γ_{US} energies, respectively [72]. It is critical to obtain reasonable values of the unstable stacking fault energy as this parameter has been tied to the mechanics and nucleation of dislocations [67]; hence this Ni potential was used to generate the MD simulations for dislocation nucleation and penetration of GBs (Fig. 6). The anti-phase boundary energy is calculated using the EAM potential for Ni–Al in the $L1_2$ structure [73], each of which gives very good agreement with the individual stacking fault energies for Ni and Al, although the APB energy is slightly higher compared to experimental and ab initio results for the ordered Ni_3Al intermetallic [74] (Fig. 7e).

3.3. Failure criterion and test cases

Remaining consistent with the other historical energy balances [40–45,63–67], we check the stability of the PSB by differentiating with respect to plastic deformation, specifically movement of the glissile dislocations. Each component of the energy balance in Eq. (1) is expressed as an increment of slip, ∂X_i, thus making differentiation very amenable and computationally efficient. The minimum energy of the PSB is determined:

$$\frac{\partial E}{\partial X_i} = 0. \tag{22}$$

Additionally, the second derivative of the energy must be positive to ensure that the energy corresponds to a local stable minimum. Thus, we establish Eq. (22) as our failure criterion for fatigue crack initiation corresponding to stability and equilibrium of the PSB's energy.

Hence, this model sums the energy contributions of each term in Eq. (1) within the grain most likely to form a PSB (favorable energy for failure based on a combination of orientation, grain size and adjacent grain boundary character–CSL Σ values). This energy balance evolves with increasing loading cycles; meanwhile physically there is significant irreversible slip within the PSB, leading to dislocations penetrating the GB, thereby forming extrusions. When the PSB achieves stability, i.e. it reaches a minimum energy configuration, a crack initiates from the PSB. The crack nucleates at the site of the extrusions (ledge and step features) at the intersection of the PSB and GB.

Various test cases at a series of total applied strain ranges, $\Delta\varepsilon^a$, were created to check this model for trends such as grain sizes, CSL Σ values and Schmid factors.

Table 1
Fatigue model test cases results showing the cycles to crack initiation for various applied strain ranges based on deviations in the microstructure (grain sizes, CSL Σ values, and Schmid factors).

	Case 1	Case 2	Case 3	Case 4	Case 5	Case 6	Case 7	Case 8
Grain size (μm)	2	2	4	4	2	2	4	4
CSL sigma value, Σ	7	7	7	7	9	9	9	9
Energy ratio (from Σ)	3.63	3.63	3.63	3.63	1.16	1.16	1.16	1.16
Schmid factor	0.3	0.42	0.3	0.42	0.3	0.42	0.3	0.42
N_i for $\Delta\varepsilon^a = 1.30\%$	13,247	6459	11,152	5428	8143	3965	3259	6700
N_i for $\Delta\varepsilon^a = 1.20\%$	18,800	9171	15,831	7711	11,574	5647	4643	9526
N_i for $\Delta\varepsilon^a = 1.10\%$	28,319	13,986	23,877	11,786	17,581	8757	7230	14,501
N_i for $\Delta\varepsilon^a = 1.00\%$	44,862	22,207	37,845	18,727	27,926	13,976	11,552	23,049
N_i for $\Delta\varepsilon^a = 0.95\%$	58,982	30,874	50,019	26,298	37,993	20,687	17,393	31,644
N_i for $\Delta\varepsilon^a = 0.90\%$	132,615	83,150	114,651	73,165	95,537	65,241	57,564	82,097

The microstructure features of the grain within the polycrystal in which a PSB forms is shown in Table 1 for each test case along with the resulting cycles until crack initiation. The results are plotted in Fig. 8 in a typical strain–life format. From these test cases, we can observe the variation in fatigue life by changing a single parameter. Hence, changing the grain size from 2 to 4 μm results in a reduction in fatigue life as shown by the differences in the blue to gray and similarly red to black curves (both solid and dashed lines) in Fig. 8: we can see that smaller grains exhibit a longer fatigue life as expected from the literature [1–7].

In addition, we see that the crack initiation life is significantly affected by varying the character of the GB, which is intersected by a PSB, resulting in formation of a static extrusion at the GB. In Table 1, we display the result of two CSL Σ values: $\Sigma7$ and $\Sigma9$. In these cases, the $\Sigma7$ GB corresponds to a 38.2° twist rotation about the $\langle 1\,1\,1\rangle$ axis and a relatively low energy of 503.5 mJ m^{-2}, meanwhile the $\Sigma9$ GB is a 38.94° tilt rotation about the $\langle 1\,1\,0\rangle$ axis resulting in a significantly higher energy of 932.2 mJ m^{-2}. For the purpose of our code, the activation energy ratios as expressed in Eqs. (10) and (20) for the $\Sigma7$ and $\Sigma9$ GBs are 3.63 and 1.16, respectively; in this case the ratio refers to the activation energy value in comparison to the saturation values shown in Fig. 6. Hence the result of varying the GB character from $\Sigma7$ and $\Sigma9$ is seen by comparing the solid to dashed lines of similar color in Fig. 8. The lower static energy GB ($\Sigma7$) offers a longer life, since it offers more resistance to slip nucleation/penetration thus hindering crack initiation; this is in agreement with early work [11–13] suggesting that GBs with low Σ values do not crack during fatigue testing. As expected, the most significant factor is the grain orientation: changing the Schmid factor from 0.3 to 0.42 results in substantial life degradation as shown by comparisons of the blue to red and gray to black curves (both solid and dashed lines) in Fig. 8.

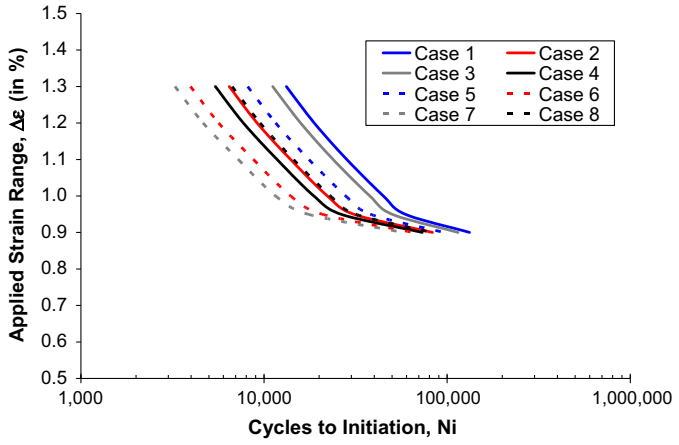

Fig. 8. Strain–life curve for predicting crack initiation based on our physically based fatigue model. The various curves represent test cases as described in Table 1.

Each term's contribution to the energy balance along with the total energy of the PSB is shown evolving with applied loading cycles in Fig. 9. The values plotted are the derivative of each energy term with respect to an increment of slip. The test case in this plot refers to a microstructure with a grain size of 2 μm, Schmid factor of 0.3 and $\Sigma7$ GB character at total applied strain ranges, $\Delta\varepsilon^a$, of 1.30% and 0.90%, resulting in a crack initiating at 13,247 and 132,615 cycles, respectively. As discussed, the continuum terms (i.e. the first three terms of Eq. (1)) provide a stress field that must be overcome for slip within the PSB. Consistent with traditional energy balances, the external work opposes the PSB energy formation, hence this value is subtracted in the energy balance (Eq. (3)), resulting in a negative value of the blue line in Fig. 9. The sharp kink in the blue line occurs upon saturation of the dislocation density and the material hardening stress response to the applied external strain. The dashed lines represent dislocations cutting through the γ matrix and the γ' precipitates to form the PSB, which remain relatively constant throughout fatigue loading. The cyan curve represents the energy of dislocations nucleating from the GB and forming within the PSB. This value increases slightly as the dislocation density increases, although its low value in this case is representative of the high energy barrier caused by the $\Sigma7$ GB. For other GBs, the energy from dislocation nucleation can be quite substantial. Physically, cracks initiate at the extrusions (i.e. ledges/steps) across the GB, hence it is reassuring that this corresponding energy drives the energy balance. Dislocations pile-up at the GB and eventually penetrate the GB, forming extrusions, at which point the energy increases substantially as

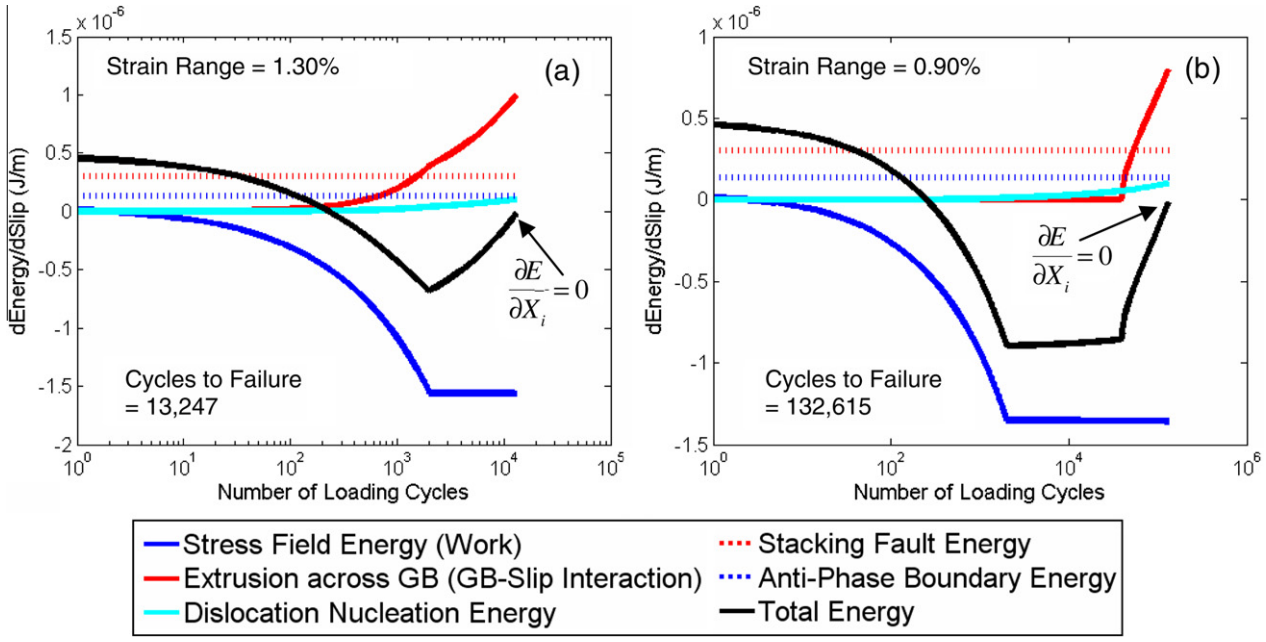

Fig. 9. The evolution of the individual and total energy components from our energy balance (Eq. (1)) with increasing loading cycles; each term is expressed as a derivate with respect to a slip increment. Hence, the total energy (black line) reaches a minimum as its derivate approaches zero, which is defined as stability of the PSB and crack initiation. The two plots are shown for strain ranges of (a) 1.30% and (b) 0.90%.

shown by the red curve. The black curve represents the total energy of the system, which is the sum of all other curves. This value is initially dominated by the applied work and later balanced by the extrusion energy. Once again, each of these curves represents the derivative with respect to a slip increment. Hence, as the black curve approaches zero, this corresponds to stability of the PSB and is our criterion for crack initiation. Attention must be paid to ensure that the stability refers to a minimum energy configuration of the PSB, hence the derivative of the total energy is zero and its second derivative is positive; in Fig. 9, this occurs the second time the black curve reaches zero.

4. Discussion

This model is physically based, and thus incorporates the microstructure of the material, which provides an attractive solution to material failure. Moreover, the model sums the individual contributions to the PSB's energy, as PSBs have been observed in this material as a consequence of fatigue loading. As the PSB energy reaches a stable configuration and a minimum value, a crack initiates at the extrusion resulting from the penetration of the PSB across a GB. It is noteworthy that this physically based model displays the correct trends for grain size, grain orientation (Schmid factor), GB character (CSL Σ value) and volume fraction of γ' precipitates as well as the familiar curvature of the strain–life plot. We analyzed the sensitivity of the microstructural variables on the model's prediction for cycles to crack initiation as shown in Fig. 10.

The grain size sensitivity results showed that decreasing the grain size from 30 to 1 μm resulted in an approximately 5.3× increase in life until crack initiation as shown in Fig. 10a. Although experimental data is not readily available on U720, this trend (i.e. decrease in grain size leading to longer fatigue life) is seen in the literature, as previously discussed [1–7]. Lukas and Kunz observed a fatigue life increase of ~3× (at a medium $\Delta\varepsilon^a$) by decreasing the grain size by a factor of ~17× in copper [5]. Our model predicts an increase in fatigue life of 2.94–3.17× for a similar decrease in grain size. Thus, the trends and magnitudes that our fatigue model predicts seem reasonable; in addition, our model predicts that PSBs form in the larger grains in a polycrystal with a wide distribution of grain sizes, as observed for a variety of materials [8–10] including Ni-based superalloys [75]. The grain size dependency is inherent to our model: each term essentially involves an energy density, which must be multiplied by the volume of the PSB to obtain the energy. Since PSBs span the entire length of the grain, there is thus a grain size dependency in each term. For the energy to nucleate dislocations from the GB and accumulate in the PSB, the length scale dependency is squared. Since the energy density is proportional to the number of dislocations in the PSB, in order to find this quantity, the dislocation density, ρ, must be multiplied by the area of the PSB (hL).

Likewise, an approximately 2.6× increase in fatigue life was observed by changing the Schmid factor from 0.50 to 0.25 in the grain orientation sensitivity chart in Fig. 10b. Thus, higher Schmid factors (more favorable orientations) are prone to PSB formation and shorter fatigue life. This trend has been confirmed by experiments reported in the literature [9,35–38,75]. Experiments cannot quantifiably describe a one-to-one relationship between Schmid factor and fatigue life: this type of

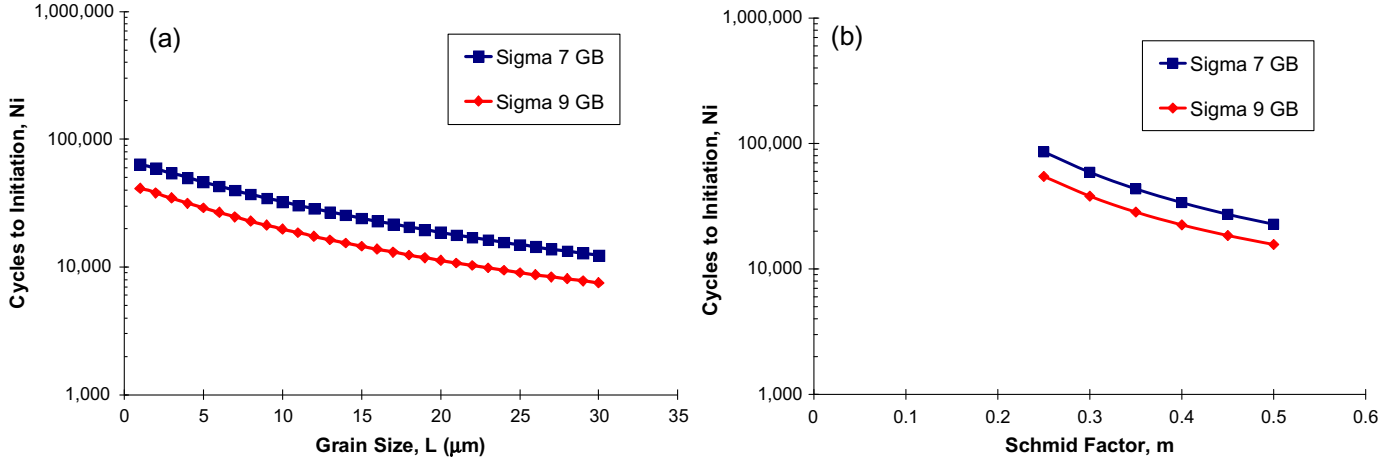

Fig. 10. Sensitivity analysis of the model based on varying the input factors for (a) grain size, L, and (b) Schmid factor, m, for PSBs forming extrusions across $\Sigma 7$ and $\Sigma 9$ GBs. For these test cases, the applied strain range is 0.95%.

unique relationship is only established through a model with predictive capabilities. To establish the model's relationship with the Schmid factor, we must analyze the individual terms. The continuum stress field is linearly dependent on the Schmid factor, since there is a direct correlation between the grain orientation and resulting number of dislocations. Further, both the dislocation nucleation and extrusion energy terms are proportional to the Schmid factor squared as previously discussed, thus controlling the relationship.

As seen in Fig. 10, by changing the character of the GB from $\Sigma 9$ to $\Sigma 7$, the fatigue life increased by approximately 55%. The dominating terms controlling this behavior were the dislocation nucleation and extrusion energy: both had an exponential dependence on the activation energy barrier presented by the character of the GB. In this simulation, the exponential relationship was expanded by a Taylor series, in which terms greater than third-order were discarded. Once again, it is difficult to establish bicrystals of U720 to experimentally depict this trend. Thus, we must rely on the model's prediction and confirm this behavior from the literature. Many experimental studies have suggested that lower-energy CSL boundaries resist cracking and have an extended fatigue life [11–13].

Furthermore, each term in this analysis is seen to saturate except for the extrusion energy. Hence, during the fatigue process, there is a dynamic equilibrium between dislocation nucleation and annihilation, which results in the dislocation density reaching a nearly constant value. The saturation of the dislocation density evolution represents irreversibility within the fatigue model. At the saturation point, the number of dislocations that are generated and annihilated are approximately equivalent. Thus, the dislocation nucleation energy, applied stress, dislocation pile-up energy, work-hardening and energy associated with slip (APB and SF) also reach a constant value in our model. However, during this saturation process, dislocations still flow within the PSB, resulting in extrusions at the GB, hence the extrusion energy is the only term in our energy balance that does not saturate.

The back-stress that the material experiences during the unloading portion of fatigue is taken into account from the internal stress field created by the pile-up of dislocations, applied loading and work-hardening of the system. Additionally, this model can be amended to account for fatigue loading with various R-ratios (mean stresses). The application of normal loading has been shown to affect the stacking fault energy curve [76], and thus has a significant impact on the response of each of the terms established by atomic simulations (i.e. the last four terms in Eq. (1)). Further, we would like to reiterate that U720, a wrought Ni-based superalloy, was chosen to display our model's effectiveness due to the complexities and vast distributions of features in the material's microstructure. The concepts presented in this model are general for fatigue in any pure metal or alloy whose failure mechanism is attributed to slip localization in the form of PSBs; thus this model can predict fatigue crack initiation for wide range of materials.

5. Conclusions

This study represents a substantial effort in the field of physically based fatigue modeling. The major contributions are as follows:

- Through optical microscopy and TEM imaging, the fatigue crack initiation mechanism in U720 is experimentally observed to be transgranular facets formed from PSBs.
- The contributing elements to the energy of the PSB were identified. In order for plastic deformation to occur within the PSB, a dislocation must glide within a stress field established by the dislocation pile-up, work-hardening of the material and applied stress. Additionally, the energy barriers for dislocations to nucleate from and penetrate a GB were determined from MD

simulations. These MD contributions serviced our model as the γ matrix/γ′ precipitates were sheared, dislocations nucleated/collected within the PSB, and extrusions formed at the intersection of the PSB and GB.
- The aforementioned terms were expressed in an energy balance for the total energy of the PSB, which evolved with increasing fatigue cycles. The stability of the PSB corresponded to a minimum value of the energy balance, which was computed as the derivative of the total PSB energy with respect to plastic deformation (i.e. an increment of slip) reaching zero, which is consistent with other historical energy balance approaches.
- This methodology is attractive since it is physically based and inherently accounts for the microstructure of the material. This result produces the correct trends for predicting fatigue crack initiation based on total applied strain range, grain size, grain orientation, GB character (CSL Σ value) and volume fraction of γ′ precipitates—all of which have a significant impact on the fatigue life of the material.

Acknowledgments

Support for this work was provided by Rolls-Royce Corporation and the National Science Foundation, DMR 08-03270.

Appendix A

MD simulations were created to reconstruct CSL Σ GBs from distinct orientations of crystal lattices consisting of fcc Ni using the Foiles–Hoyt potential [71]. The simulation box was deformed using an *NPT* ensemble with periodic boundary conditions. A void was introduced into the system to facilitate dislocation nucleation leading to slip–GB interaction. To grasp the role of the GBs on the energetics of each system, the potential energy of each atom was measured during the simulation. A control box was placed at the intersection of the dislocation and GB along the atoms which play a role in the interaction (selected via the centrosymmetry parameter [77]); hence it is not a simple cubic box. Extreme care was taken to select the positions of only the relevant defect atoms to determine the energy upon loading of that atom, which was reduced by the energy of that atom in its static relaxed position and normalized by the volume of the control box. In order to verify these MD calculations for determining the energy barrier, a system was constructed without a GB to mimic slip in an fcc lattice. The result of our MD control box method was compared to the generalized stacking fault energy and produced a modest 6% difference, thus validating this procedure.

This procedure was repeated for various CSL Σ GBs, in order to measure the energy barrier for slip transmission: $\langle 1\,1\,0\rangle$ tilt – Σ3, 9, 11, 17, 19; $\langle 1\,1\,1\rangle$ twist – Σ3, 7, 13, 21; and $\langle 0\,0\,1\rangle$ tilt – Σ5. Similarly, the void was removed from our MD system and the simulation box was deformed to measure the energy barriers associated with slip nucleation from the GB. The Σ3 and Σ11 GBs have a stable configuration; hence nucleation from the GB was not observed in the simulation. We rationalized the energy barriers for various types of GB with their static GB energy. The results of this process are shown in Fig. 6 as the energy barrier for slip nucleating from a GB and slip transmission across a GB is plotted against the static GB energy for each GB. There is an inverse relationship between the energy barrier against slip and static energy for each type of GB. A power-law function was fitted to the data, resulting in Eqs. (15) and (17), respectively. Details concerning the methodology of these MD simulations and a discussion of the results can be found in Ref. [70].

In this section, we offer a simulation-based approach for obtaining the energy barriers associated with slip transmission/nucleation from a GB: this information is extremely hard to obtain experimentally and no such analytical model can be developed (due to the complexity of certain GB types). We have calculated these energy barriers for multiple cases using atomistic simulations and generalized this approach by applying a fit to the results. This methodology offers substantial progress compared to other types of models, which approximate or back-fit (from experiments) these energy barrier values without distinguishing different GB types. Hence in doing so, we can locally/spatially evaluate the energy barriers for individual GBs, which are of particular interest for fatigue crack initiation modeling.

References

[1] Sinclair GM, Craig WJ. Influence of grain size on work hardening and fatigue characteristics of alpha brass. Cleveland (OH): American Society of Metals; 1952. p. 18.
[2] Thompson AW. Scripta Metall 1971;5:859.
[3] Thompson AW, Backofen WA. Acta Metall 1971;19:597.
[4] Thompson AW, Backofen WA. Metall Mater Trans A: Phys Metall Mater Sci 1971;2:2004.
[5] Lukas P, Kunz L. Mater Sci Eng 1987;85:67.
[6] Morrison DJ, Moosbrugger JC. Int J Fatigue 1997;19:S51.
[7] Liu HW. Int J Fract 1999;96:331.
[8] Weidner A, Beyer R, Blochwitz C, Holste C, Schwab A, Tirschler W. Mater Sci Eng A: Struct Mater: Properties, Microstruct Process 2006;435–436:540.
[9] Buque C, Bretschneider J, Schwab A, Holste C. Mater Sci Eng A: Struct Mater: Properties, Microstruct Process 2001;A319–321:631.
[10] Keller R, Zielinski W, Gerberich WW. Mater Sci Eng A 1989;A113:267.
[11] Lim LC. Acta Metall 1987;35:1653.
[12] Pan Y, Adams BL, Olson T, Panayotou N. Acta Mater 1996;44:4685.
[13] Field DP, Adams BL. Acta Metall Mater 1992;40:1145.
[14] Polak J. Scripta Metall 1970;4:761.
[15] Basinski ZS, Basinski SJ. Prog Mater Sci 1992;36:89.
[16] Ewing JA, Humfrey JCW. Philos Trans Roy Soc Lond Ser A 1903;200:241 [Containing papers of a mathematical or physical character].
[17] Seeger A, Diehl J, Mader S, Rebstock H. Philos Mag 1957;2:323.
[18] Friedel J. Proc Roy Soc Lond, Ser A: Math Phys Sci 1957;242:145.
[19] Christ HJ. Cyclic stress-strain response and microstructure. Fatigue and fracture, vol. 19. ASM Handbook; 1996. p. 73.
[20] Grosskreutz JC. Phys Status Solidi B 1971;47:11.

[21] Grosskreutz JC. Phys Status Solidi B 1971;47:359.
[22] Basinski ZS, Basinski SJ. Scripta Metall 1984;18:851.
[23] Hunsche A, Neumann P. Acta Metall 1986;34:207.
[24] Ma B-T, Laird C. Acta Metall 1989;37:325.
[25] Ma B-T, Laird C. Acta Metall 1989;37:337.
[26] Essmann U, Gosele U, Mughrabi H. Philos Mag A: Phys Conden Matter, Defects Mech Properties 1981;44:405.
[27] Differt K, Essmann U, Mughrabi H. Philos Mag A: Phys Conden Matter, Defects Mech Properties 1986;54:237.
[28] Essmann U, Mughrabi H. Philos Mag A: Phys Conden Matter, Defects Mech 1979;40:731.
[29] Mughrabi H, Wang R, Differt K, Essmann U. Fatigue crack initiation by cyclic slip irreversibilities in high-cycle fatigue. Dearborn. MI: ASTM; 1983. p. 5.
[30] Kuhlmann-Wilsdorf D, Laird C. Mater Sci Eng 1977;27:137.
[31] Kuhlmann-Wilsdorf D. Mater Sci Eng A 1989;A113:1.
[32] Brown L. Dislocation and the fatigue strength of metals. In: Ashby M, Bullough R, Hartley C, Hirth J, editors. Dislocation modelling of physical systems: proceedings of the acta-scripta metallurgica conference. Oxford: Pergamon Press; 1980. p. 51.
[33] van der Giessen E, Needleman A. Modell Simul Mater Sci Eng 1995;3:689.
[34] Brinckmann S. On the role of dislocations on fatigue crack initiation. PhD thesis, Zernike Institute for Advanced Materials, University of Groningen, Netherlands; 2005. <http://homepage.ruhr-uni-bochum.de/steffen.brinckmann/WORK/DDD/index.html>.
[35] Mughrabi H, Wang R. Cyclic deformation of face-centered cubic polycrystals: a comparison with observations on single crystals. In: Hansen N, Horsewell A, Leffers T, Lilholt H, editors. Deformation of polycrystals: mechanisms and microstructure. Proceedings, second risø international symposium on metallurgy and materials science. Roskilde, Denmark: Risø National Laboratory; 1981. p. 87.
[36] Winter AT, Pedersen OR, Rasmussen KV. Acta Metall 1981;29:735.
[37] Buque C. Int J Fatigue 2001;23:459.
[38] Buque C, Bretschneider J, Schwab A, Holste C. Mater Sci Eng A 2001;300:254.
[39] Lin TH, Ito YM. J Mech Phys Solids 1969;17:511.
[40] Tanaka K, Mura T. J Appl Mech 1981;48:97.
[41] Lin MR, Fine ME, Mura T. Acta Metall 1986;34:619.
[42] Tanaka K, Mura T. Mech Mater 1982;1:63.
[43] Mura T, Nakasone Y. Trans ASME. J Appl Mech 1990;57:1.
[44] Venkataraman G, Chung YW, Nakasone Y, Mura T. Acta Metall Mater 1990;38:31.
[45] Mura T. Mater Sci Eng A 1994;A176:61.
[46] Kruml T, Polak J, Obrtlik K, Degallaix S. Acta Mater 1997;45:5145.
[47] Petersmeier T, Martin U, Eifler D, Oettel H. Int J Fatigue 1998;20:251.
[48] Chieragatti R, Remy L. The low cycle fatigue behaviour of MAR-M200 single crystals at 650C. Amsterdam: Elsevier; 1988. p. 133.
[49] Stoltz RE, Pineau AG. Mater Sci Eng 1978;34:275.
[50] Fritzemeier LG, Tien JK. Acta Metall 1988;36:275.
[51] Clavel M, Pineau A. Scripta Metall 1982;16:361.
[52] Alexandre F, Deyber S, Pineau A. Scripta Mater 2004;50:25.
[53] Petrenec M, Obrtlik K, Polak J. Mater Sci Eng A 2005;400–401:485.
[54] Petrenec M, Obrtlik K, Polak J, Man J. Key Eng Mater 2007:383.
[55] Petrenec M, Obrtlik K, Polak J, Man J. Mater Sci Forum 2008;567–568:429.
[56] Risbet M, Feaugas X, Guillemer-Neel C, Clavel M. Scripta Mater 2003;49:533.
[57] Risbet M, Feaugas X. Eng Fract Mech 2008;75:3511.
[58] Huang EW, Barabash RI, Yandong W, Bj C, Li L, Liaw PK, et al. Int J Plast 2008;24:1440.
[59] Sangid MD, Sehitoglu H, Maier HJ, Niendorf T. Mater Sci Eng A 2010;527:7115.
[60] Ren W, Nicholas T. Mater Sci Eng A 2002;332:236.
[61] Joyce MR, Reed PAS. Fatigue crack growth behaviour under mixed mode loading in udimet 720 SX. Champion (PA): Minerals, Metals and Materials Society; 2004. p. 295.
[62] Pang HT, Reed PAS. Int J Fatigue 2008;30:2009.
[63] Griffith AA. Roy Soc Lond – Philos Trans 1920;221:163.
[64] Cooper RE. Acta Metall 1965;13:46.
[65] Cooper RE. Acta Metall 1966;14:78.
[66] Rice JR, Thomson R. Philos Mag 1974;29:73.
[67] Rice JR. J Mech Phys Solids 1992;40:239.
[68] Eshelby JD, Frank FC, Nabarro FRN. Philos Mag 1951;42:351.
[69] Argon AS. Strengthening mechanisms in crystal plasticity. Oxford: Oxford University Press; 2008.
[70] Sangid MD, Ezaz T, Sehitoglu H, Robertson IM. Acta Mater, 2010; in press, doi:10.1016/j.actamat.2010.09.032.
[71] Foiles SM, Hoyt JJ. Acta Mater 2006;54:3351.
[72] Siegel DJ. Appl Phys Lett 2005;87:121901.
[73] Mishin Y. Acta Mater 2004;52:1451.
[74] Sun Y, Rice JR, Truskinovsky L. Dislocation nucleation versus cleavage in Ni_3 Al and Ni. Pittsburgh (PA): Materials Research Society; 1991. p. 243.
[75] Miao J, Pollock TM, Wayne Jones J. Acta Mater 2009;57:5964.
[76] Tschopp MA, McDowell DL. J Mech Phys Solids 2008;56:1806.
[77] Kelchner CL, Plimpton SJ, Hamilton JC. Phys Rev B: Condens Matter 1998;58:11085.